Published OnlineFirst January 10, 2020; DOI: 10.1158/1535-7163.MCT-19-0695

Preclinical Activity of Ribociclib in Squamous Cell Carcinoma of the Head and Neck

Gabrielle van Caloen[1], Sandra Schmitz[1,2,3], Mariama El Baroudi[1], Xavier Caignet[1], Sébastien Pyr dit Ruys[4], Pierre P. Roger[5], Didier Vertommen[4], and Jean-Pascal Machiels[1,2,3]

ABSTRACT

Cell-cycle pathway impairments resulting in CDK4 and 6 activation are frequently observed in human papillomavirus (HPV)-negative squamous cell carcinoma of the head and neck (SCCHN). We investigated the activity of ribociclib, a CDK4/6 inhibitor, in SCCHN models with the aim of identifying predictive biomarkers of response. HPV-negative or HPV-positive SCCHN cell lines ($n = 8$) and patient-derived tumor xenograft (PDTX) models ($n = 6$) were used. The models were classified according to their sensitivity to ribociclib to investigate potential predictive biomarkers. Ribociclib had a cytostatic effect in some HPV-negative SCCHN models but had no effect in HPV-positive models. In SCCHN cell lines and PDTXs, the retinoblastoma (Rb) protein expression level correlated with ribociclib activity. Rb knockdown was, however, not sufficient to block G_0–G_1 arrest induced by ribociclib in Detroit-562 where p107, p130, and Forkhead BOX M1 (FOXM1) were also implicated in ribociclib activity. Cell lines harboring epithelial-to-mesenchymal transition (EMT) features were less sensitive to ribociclib than those with an epithelial phenotype. Rb downregulation induced EMT in our Rb-expressing SCCHN cell lines. However, ribociclib still had significant activity in one PDTX model with high Rb and vimentin expression, suggesting that the presence of vimentin alone is not enough to induce ribociclib resistance. These findings suggest that CDK4/6 inhibitors should be investigated in patients with HPV-negative SCCHN with high Rb expression and an epithelial phenotype. Although these biomarkers are not predictive in all cases, they may enrich the population that could benefit from CDK4/6 inhibitors.

Introduction

Squamous cell carcinoma of the head and neck (SCCHN) is the seventh most common cancer worldwide and is mostly due to tobacco use and/or alcohol consumption (1). The human papillomavirus (HPV) is another cause of oropharyngeal cancer (2, 3).

Single modality treatment (surgery or radiotherapy) is usually offered for early-stage tumors and provides a cure rate between 70% and 90%. Patients with locally advanced disease benefit from multimodal treatment but approximately one third will relapse (4). Median overall survival (OS) for patients with locally recurrent and/or metastatic (R/M) SCCHN remains low at around 12 to 15 months (5, 6).

HPV-positive oropharyngeal cancer is induced by the expression of the viral E6 and E7 oncoproteins, which mediate the degradation of p53 and retinoblastoma (Rb) proteins with subsequent cell-cycle progression (7). In contrast, genetic alterations implicated in the cell cycle are found in nearly every HPV-negative SCCHN and include the tumor suppressor genes *TP53* and *CDKN2A* in 84% and 58% of patients, and the amplification of the proto-oncogenes *CCND1* and *MYC* in 31% and 14%, respectively (8). These genetic aberrations strongly support the investigation of CDK4/6 inhibitors such as palbociclib or ribociclib in HPV-negative SCCHN.

Phase I/II clinical trials have demonstrated that ribociclib or palbociclib in combination with cetuximab is safe (9, 10). However, a randomized phase II trial failed to demonstrate a statistically significant benefit in progression-free survival (PFS) and overall survival (OS) of the palbociclib/cetuximab combination over cetuximab alone in unselected patients with HPV-negative SCCHN (11). Therefore, a better understanding of the molecular mechanisms involved in treatment response and/or resistance is needed to optimally select patients who could benefit from CDK4/6 inhibitors.

In this work, we investigated the activity of ribociclib in several HPV-negative and HPV-positive preclinical SCCHN models with the aim of identifying predictive biomarkers of response.

Materials and Methods

Cell lines and cell culture

Cell lines (CAL27, FaDu, Detroit-562, SCC9, SCC15, and SCC25) were purchased from the ATCC. UPCI-SCC90 was purchased from DSMZ-German collection of microorganisms and cell culture. UM-SCC47 was provided by Dr. T.E. Carey (University of Michigan, Ann Arbor, MI). Cell line identities were verified every 6 months as described by Schneider and colleagues (12), and only cells under 10 passages were used in the experiments. All cell lines were tested for *Mycoplasma* contamination with the MycoAlert Mycoplasma Detection Kit (Lonza) before being used.

[1]Institut de Recherche Clinique et Expérimentale (Pole MIRO), Université Catholique de Louvain (UCLouvain), Brussels, Belgium. [2]Institut Roi Albert II, Department of Medical Oncology, Cliniques Universitaires Saint-Luc, Brussels, Belgium. [3]Department of Head and Neck Surgery, Cliniques Universitaires Saint-Luc, Brussels, Belgium. [4]Protein Phosphorylation Unit, de Duve Institute, Université Catholique de Louvain (UCLouvain), Brussels, Belgium. [5]ULB-Cancer Research Center (U-CRC) Université Libre de Bruxelles, Brussels, Belgium.

Note: Supplementary data for this article are available at Molecular Cancer Therapeutics Online (http://mct.aacrjournals.org/).

Corresponding Author: Jean-Pascal H. Machiels, Cancer Center, Cliniques Universitaires Saint-Luc and Institut de Recherche Clinique et Expérimentale (Pole MIRO), Université Catholique de Louvain, Brussels 1200, Belgium. Phone: 322-764-5457; Fax: 322-764-5428; E-mail: jean-pascal.machiels@uclouvain.be

Mol Cancer Ther 2020;19:777–89

doi: 10.1158/1535-7163.MCT-19-0695

Published OnlineFirst January 10, 2020; DOI: 10.1158/1535-7163.MCT-19-0695

Cell viability assay by 3-(4,5-dimethylthiazol-2-yl)-2,5-diphenyltetrazolium (MTT)

Cells were seeded in 96-well plates at 3,000 cells/well and treated in triplicate for 72 hours with 12 concentrations of ribociclib ranging from 0.5 to 20 μmol/L. The viable cell number was determined by adding Dye Solution (CellTiter 96 Non-Radioactive Cell Proliferation Assay, Promega), which converts tetrazolium salt into a formazan product detected at a wavelength of 570 nm using a Benchmark Plus Microplate Spectrometer (Bio-Rad).

Cell-cycle analysis by flow cytometry

Cell-cycle analysis by bromodeoxyuridine (BrdU) incorporation was performed using the FITC BrdU Flow Kit (BD Pharmingen) according to the manufacturer's guidelines. The analysis was performed by flow cytometry (FACSCalibur, BD Biosciences) with CellQuest Pro software (BD Biosciences). The cell-cycle status was analyzed with a flow cytometer using FlowJo software vX.0.7 (Tree Star, Inc.).

Immunoblot analysis

Cells were lysed on ice for 5 minutes in lysis buffer containing Pierce RIPA buffer with 1% phosphatase inhibitor cocktail and 1% protease inhibitor cocktail (Thermo Fisher Scientific). Protein concentration was evaluated using Pierce BCA Protein Assay Kit (Thermo Fisher Scientific). The proteins were separated by SDS-PAGE electrophoresis on graduated Mini-Protean TGX 4%–15% polyacrylamide gels (Bio-Rad) and transferred to polyvinylidene difluoride membranes (Bio-Rad). The membranes were blocked with 5% milk in Tris-buffered saline, with Tween 20, pH 8.0 (Sigma Aldrich) for 1 hour at room temperature and then incubated overnight at 4°C with primary antibodies. After washing, the membranes were incubated for 1 hour at room temperature with horseradish peroxidase (HRP)-conjugated secondary antibodies (Jackson Immunoresearch). The membranes were finally incubated with HRP substrate to enhance chemiluminescence (ECL, Thermo Fisher Scientific). Chemiluminescence was then revealed by exposure to CL-Xposure Film (Thermo Fisher Scientific) incubated in Kodak developer followed by Kodak fixer (Sigma Aldrich).

Antibodies for immunoblotting were purchased from Santa Cruz Biotechnology (CDK2 #sc-6248, p107 #sc-318, p130 #sc-317, FOXM1 #sc-500), Sigma Aldrich (GAPDH #G9545), BD Pharmingen (p16 #554097), and Cell Signaling Technology [e-cadherin #3195, CDK4 #2906, CDK6 #13331, cyclin D1 #2926, Rb #9309, p-Rb (Ser807/811) #8516, snail #3879, vimentin #5741, cyclin A2 #4656, cyclin E1 #4129, zeb1 #3396, slug #9585].

Establishment of cell line xenograft and patient-derived tumor xenograft mouse models

CAL27 and SCC9 human cell line xenograft models were established with 1.5×10^6 and 1×10^6 cells, respectively, suspended in PBS (Lonza) and subcutaneously injected into nude female mice (nude female sp/sp mice, #NMRINU-F; Taconic Bioscience) in a final volume of 100 μL.

PDTX models were derived from patients with SCCHN, as described previously (13). They were either established in collaboration with Trace, the PDTX platform of Katholieke Universiteit (Leuven, Belgium; HNC002, HNC007, HNC010), or generated in our laboratory (UCLHN01, UCLHN03). In one model (HNC002 ResCTX), we induced resistance to cetuximab, an antibody against the EGFR, by treating the model weekly with 30 mg/kg of cetuximab. All models were HPV-negative except one (UCLHN03).

Mice were randomly divided into two or four groups and treated with 100 mg/kg ribociclib (daily), 30 mg/kg cetuximab (weekly), the combination of ribociclib and cetuximab (daily/weekly) or vehicles (daily/weekly). Ribociclib was administrated by oral gavage and cetuximab was administrated by intraperitoneal injection. Tumor size was measured with calipers once a week and was calculated according to the following equation:

$V\ (mm^3) = [(\text{the largest length}) \times (\text{the shortest length})^2]/2$

Animal work complied with Belgian law and all experiments were carried out in accordance with our local ethical committee (approval number: 2015/13AOU/445). Animal welfare is regularly controlled by inspections under Belgian law and all investigators performing animal work had successfully completed FELASA C training. The number of mice to be included per group was calculated as described previously (13).

RNA sequencing

Raw data of RNA sequencing (RNA-seq) for CAL27, Detroit-562, SCC9, SCC15, and SCC25 cell lines were obtained from Martin and colleagues (14).

siRNA transfection

siRNA targeting *RB1* (#L-003296-02-0005), *RBL1* (#L-003298-00-0005), *RBL2* (#L-003299-00-0005), *FOXM1* (#L-009762-00-0005), and negative control siRNA (#D-001810-01-05) were purchased from Dharmacon. Cells were transfected for 72 hours with 40 μmol/L siRNA using Lipofectamine RNAiMAX Transfection Reagent (Thermo Fisher Scientific).

Mobility assay

Cell migration ability was evaluated with a Transwell system using a multiwell plate with 24 wells and an 8.0-μm pore polyester (PET) membrane insert (Corning). Cells were washed twice and resuspended in serum free medium (50,000 cells/insert). The bottom chamber contained medium supplemented with 0.15% FBS (Thermo Fisher Scientific). Cells were incubated for 16 hours at 37°C and 5% CO_2 before being fixed with 4% formaldehyde at room temperature for 2 minutes. Cells were then permeabilized with 100% methanol and stained with 0.23% crystal violet (Sigma Aldrich) at room temperature for 30 minutes, protected from light. Nonmigrated cells were scraped off with cotton swabs and migrated cells were visualized into two random nonoverlapping fields at 5× objective and 10× eyepieces on a phase contrast microscope (Zeiss Axiovert 100; Hyland Scientific) using Microscope Software AxioVision program (Carl Zeiss).

Immunofluorescence analysis

Cells were fixed in 4% paraformaldehyde (without methanol) for 15 minutes at room temperature and then permeabilized in H_2O with 0.003% Triton X-100 (Sigma Aldrich), 0.05% FBS, 0.05% PBS for 1 hour at room temperature. Cells were incubated with primary antibodies overnight at 4°C. After PBS washing, cells were incubated for 1 hour at room temperature and protected from light with goat anti-rabbit IgG Alexa Fluor 488 or goat anti-mouse Alexa Fluor 568 (Thermo Fisher Scientific). Cells were then washed with PBS and incubated for 5 minutes at room temperature protected from light with DAPI (Agilent) for nuclear staining. Finally, cells were covered with coverslips using fluorescence mounting medium (Agilent).

Primary antibodies (e-cadherin #3195, β-catenin #2677) for immunoblotting were purchased from Cell Signaling Technology.

Published OnlineFirst January 10, 2020; DOI: 10.1158/1535-7163.MCT-19-0695

IHC on PDTX tumor samples

Immunostaining was performed as described previously by Bouzin and colleagues (15). Sections were incubated overnight at 4°C with the primary antibody (Rb: Abcam, #Ab181616, 1/1,000; vimentin: Thermo Fisher Scientific, 1/150; e-cadherin: Cell Signaling Technology, #3195, 1/1,000).

Stained tissue sections were digitalized using a SCN400 slide scanner (Leica Biosystems) at ×40 magnification. Immunostainings were analyzed using the image analysis tool TissueIA version 4.0.7 (Leica Biosystems). Rb expression was determined using a nuclear algorithm of the software and graded as negative, weak, moderate, or strong. A histoscore, with a potential range of 0–300, was calculated as follows: % weakly stained cells + (% moderately stained cells) × 2 + (% strongly stained cells) × 3. Vimentin and e-cadherin expression were determined as a percentage of the stained area. Thresholds, adjusted manually on representative stained versus not stained tissue areas, were applied for tissue and for DAB detection, using color deconvolution matrices of the software. Results were expressed as stained area (below threshold)/tissue area (15). Results are presented as mean ± SD of at least three different tumors.

Sample preparation for mass spectrometry analysis

Total protein content was quantified using Pierce BCA Protein Assay Kit (Thermo Fisher Scientific).

Two hundred micrograms of proteins were reduced and alkylated. Proteins were then precipitated using a methanol/chloroform procedure before being resuspended in 100 mmol/L ammonium bicarbonate (Sigma Aldrich). Protein digestion was performed using trypsin (Promega). Peptides were purified with a C18 5,000 mg column before proceeding further (Thermo Fisher Scientific).

Label-free differential two-dimensional liquid chromatography coupled to tandem mass spectrometry (2D-LC/MS-MS)

2D-LC-MS/MS analysis was performed essentially as described previously (16).

Briefly, after a first-dimension separation by hydrophilic interaction chromatography into 20 fractions, peptides were dissolved in solvent A [0.1% trifluoroacetic acid (TFA) in 2% acetonitrile (ACN)], directly loaded onto reverse-phase pre-column (Acclaim PepMap 100, Thermo Fisher Scientific), and eluted in backflush mode. Peptide separation was performed using a reverse-phase analytic column (Acclaim PepMap RSLC, 0.075 × 250 mm, Thermo Fisher Scientific) with a linear gradient of 4%–36% solvent B (0.1% TFA in 98% ACN) for 36 minutes, 40%–99% solvent B for 10 minutes and holding at 99% for the last 5 minutes at a constant flow rate of 300 nL/minute on an UltiMate 3000 RSC NanoHPLC System (Thermo Fisher Scientific). The peptides were analyzed by an Orbitrap Fusion Lumos Tribrid mass spectrometer (Thermo Fisher Scientific), and subjected to nanospray ionization. Intact peptides were measured in the Orbitrap at a resolution of 120,000 followed by a mass spectrometry (MS/MS) scan using a higher energy collisional dissociation setting at 35 until ion fragments were detected in the ion trap. A data-dependent procedure of MS/MS scans was applied for the top precursor ions above a threshold ion count of 5,000 in the MS survey scan with 30.0s dynamic exclusion. The total cycle time was set to four seconds. Full MS (MS1) spectra were obtained with an automatic gain control target of 400,000 ions and a maximum injection time of 50 milliseconds; MS2 (tandem MS) spectra were acquired with an AGC target of 10,000 ions and a maximum injection time of 35 milliseconds. For MS1 scans, the mass over charge scan range was 350 to 1,800. The resulting MS/MS data was processed using Sequest HT search engine within Proteome Discoverer 2.2 (Thermo Fisher Scientific) against a human protein reference database obtained from Uniprot. Trypsin was specified as a cleavage enzyme allowing up to two missed cleavages, four modifications per peptide and up to three charges. Mass error was set to 10 parts per million for precursor ions and 0.5 kDa for fragment ions. Oxidation on methionine, phosphorylation on serine, threonine and tyrosine were considered as variable modifications. False discovery rate (FDR) was assessed using Percolator (Thermo Fisher Scientific), and thresholds for protein, peptide and modification sites were specified at 1%. Results were analyzed using Pathway Studio (Elsevier).

Statistical analysis

Statistical analyses were performed with Prism 7 (GraphPad Software Inc.) and R (version 3.5.1, http://www.R-project.com).

To compare two independent groups, the unpaired Student *t* test was used where a $P < 0.05$ was considered to be statistically significant. To compare the effect of ribociclib, or the downregulation of Rb with the control group in SCCHN cell lines, the paired Student *t* test was also used and a $P < 0.05$ was considered to be statistically significant.

We used the freely available R/Bioconductor package DESeq (17) to analyze the differential expression of genes between the sensitive cell lines (CAL27, Detroit-562) and those less sensitive (SCC25, SCC9, SCC15) to ribociclib treatment. We used the Benjamini–Hochberg method for multiple hypothesis correction, with a significance threshold of fold change 2 and a FDR of ≤ 0.05. We used the Corrplot R package (18) to calculate the Pearson correlation coefficients between the expression levels of *RB1*, epithelial marker (*CDH1*), and mesenchymal markers (*ZEB1, TWIST1, FN1, VIM* and *SNAI2*) based on mRNA expression from RNA-seq of CAL27, Detroit-562, SCC9, SCC15, and SCC25 cell lines.

Two-way ANOVA analyzes (fixed effects: time and group) with Tukey correction for multiple *post test* comparisons were performed to compare the tumor growth of SCCHN xenografts in PDTXs.

Results

Ribociclib is cytostatic in human HPV-negative SCCHN preclinical models

Cell viability (**Fig. 1A**) and cell-cycle (**Fig. 1B** and **C**) analyses were performed in six HPV-negative (FaDu, CAL27, Detroit-562, SCC9, SCC15, SCC25) and two HPV-positive (UM-SCC47, UPCI-SCC90) human SCCHN cell lines.

On the basis of the viability assay, IC_{50} was calculated for each cell line treated with ribociclib. In HPV-negative cell lines, the IC_{50} of CAL27, FaDu and Detroit-562 was significantly lower (12.106 ± 0.901 μmol/L) than that of SCC25, SCC9, and SCC15 (19.791 ± 3.498 μmol/L; $P = 0.001$; **Fig. 1A**). HPV-positive cell lines were extremely resistant to ribociclib as even at a very high concentration of ribociclib (20 μmol/L) their IC_{50} was not reached (Supplementary Fig. S1).

Cell-cycle analysis showed that ribociclib induces arrest in the G_0–G_1 phase. In HPV-negative cell lines, this effect was dose-dependent with greater G_0–G_1 arrest seen with ribociclib 0.5 μmol/L (**Fig. 1B**) compared with 0.05 μmol/L (**Fig. 1C**). At the lower concentration (ribociclib 0.05 μmol/L), a significant arrest in G_0–G_1 compared with controls was observed in FaDu, CAL27, and Detroit-562 but not in SCC25, SCC9, and SCC15. Ribociclib did not induce cell-cycle arrest in HPV-positive SCCHN cell lines even at the highest concentration (ribociclib 0.5 μmol/L).

Therefore, based on cell viability and cell-cycle analyses, we classified these SCCHN lines into three distinct groups: sensitive HPV-

Published OnlineFirst January 10, 2020; DOI: 10.1158/1535-7163.MCT-19-0695

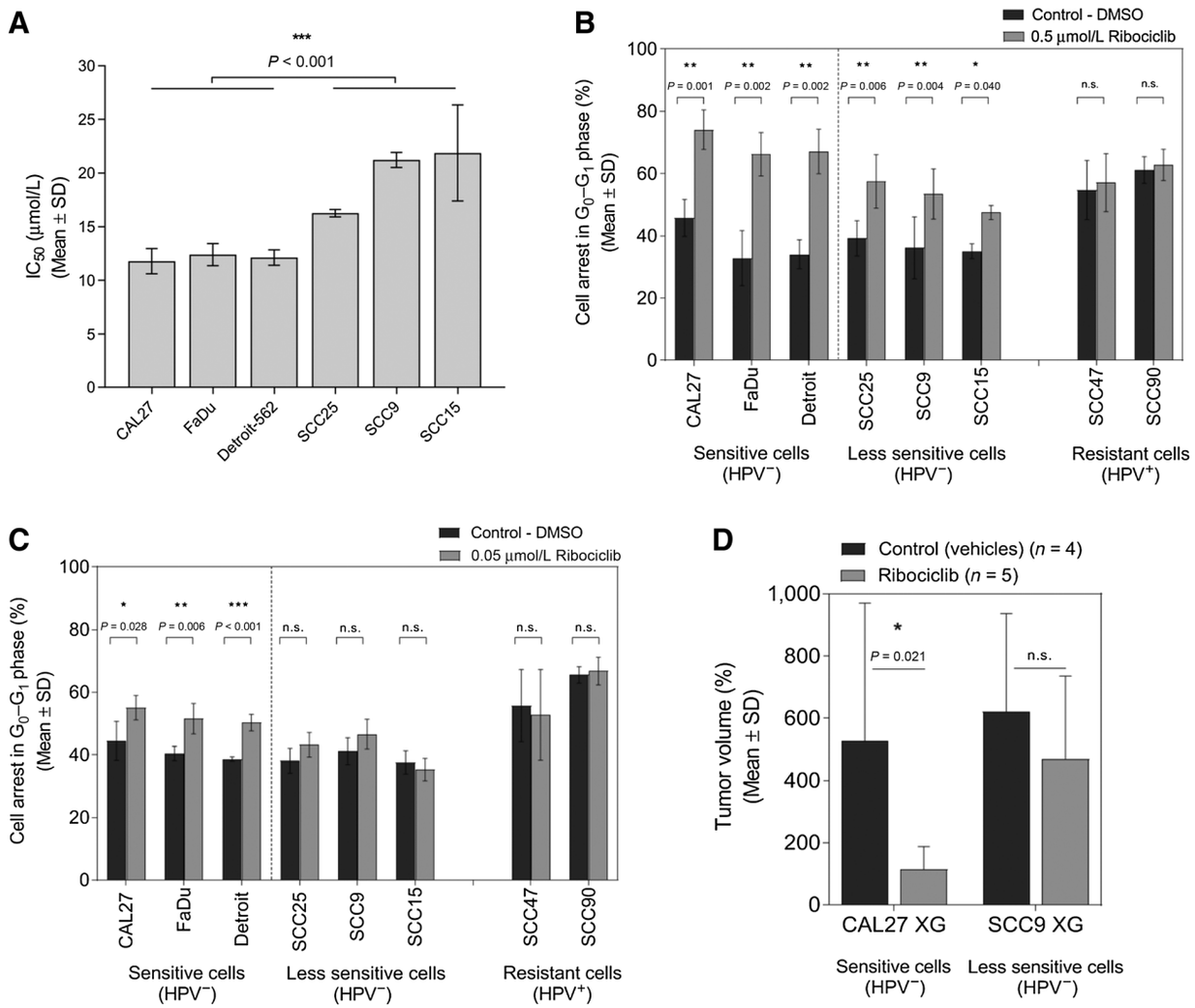

Figure 1.

Activity of ribociclib in preclinical SCCHN human models. **A,** IC_{50} values of six HPV-negative SCCHN cell lines treated for 72 hours with increasing doses of ribociclib (0.5–20 μmol/L). IC_{50} of HPV-positive cell lines was not reached (Supplementary Fig. S1). Mean ± SD were obtained in three independent MTT assays. Percentage of cell arrest in G_0–G_1 after 24 hours of treatment with 0.5 μmol/L (**B**) or 0.05 μmol/L ribociclib (gray bars) or 0.1% DMSO (black bars; **C**). Mean ± SD were obtained in three independent BrdU assays. **D,** Mice were subcutaneously implanted with CAL27 or SCC9 cells and treated daily with 100 mg/kg ribociclib (gray bars, $n = 5$) or with the vehicle (black bars, $n = 4$) for 14 days. Values represent mean ± SD. n.s.: $P > 0.05$; $^*P < 0.05$; $^{**}P < 0.001$; $^{***}P < 0.0001$. n.s., no significance.

negative cell lines (FaDu, CAL27, and Detroit-562), less sensitive HPV-negative cell lines (SCC25, SCC9, and SCC15), and HPV-positive cell lines that were resistant to ribociclib (UM-SCC47 and UPCI-SCC90; **Fig. 1A–C**). To confirm this classification, mice were subcutaneously implanted with CAL27 (sensitive) and SCC9 (less sensitive) cells (**Fig. 1D**). Ribociclib significantly reduced tumor growth in comparison with controls in the CAL27 xenograft model but not in the SCC9 xenograft model.

The activity of ribociclib was next investigated *in vivo* using six PDTX mouse models (**Fig. 2**). Tumor size stabilization was observed in three HPV-negative PDTX models (HCN002_ResCTX, HNC002, and HNC010). Tumor growth was delayed in UCLHN01 (HPV-negative) compared with controls. However, in UCLHN01, the tumor volume increased over time under ribociclib treatment. HNC007 (HPV-negative) and UCLHN03 (HPV-positive) were both resistant to ribociclib.

These data showed that ribociclib had a cytostatic effect in some HPV-negative SCCHN preclinical models and no effect in HPV-positive models.

Mesenchymal markers are expressed in less sensitive HPV-negative cell lines

To understand what determines tumor sensitivity to ribociclib exposure, we first investigated the differences in cellular and molecular phenotypes between HPV-negative SCCHN cell lines.

Interestingly, the two less sensitive HPV-negative cell lines (SCC9, SCC15) harbored a mesenchymal-like morphology compared with sensitive cell lines (CAL27, FaDu, Detroit-562) that present an epithelial-like morphology (**Fig. 3A**). Moreover, protein expression levels of vimentin and snail, two mesenchymal markers, were significantly higher in the mesenchymal-like cells (SCC9 and SCC15), compared

Published OnlineFirst January 10, 2020; DOI: 10.1158/1535-7163.MCT-19-0695

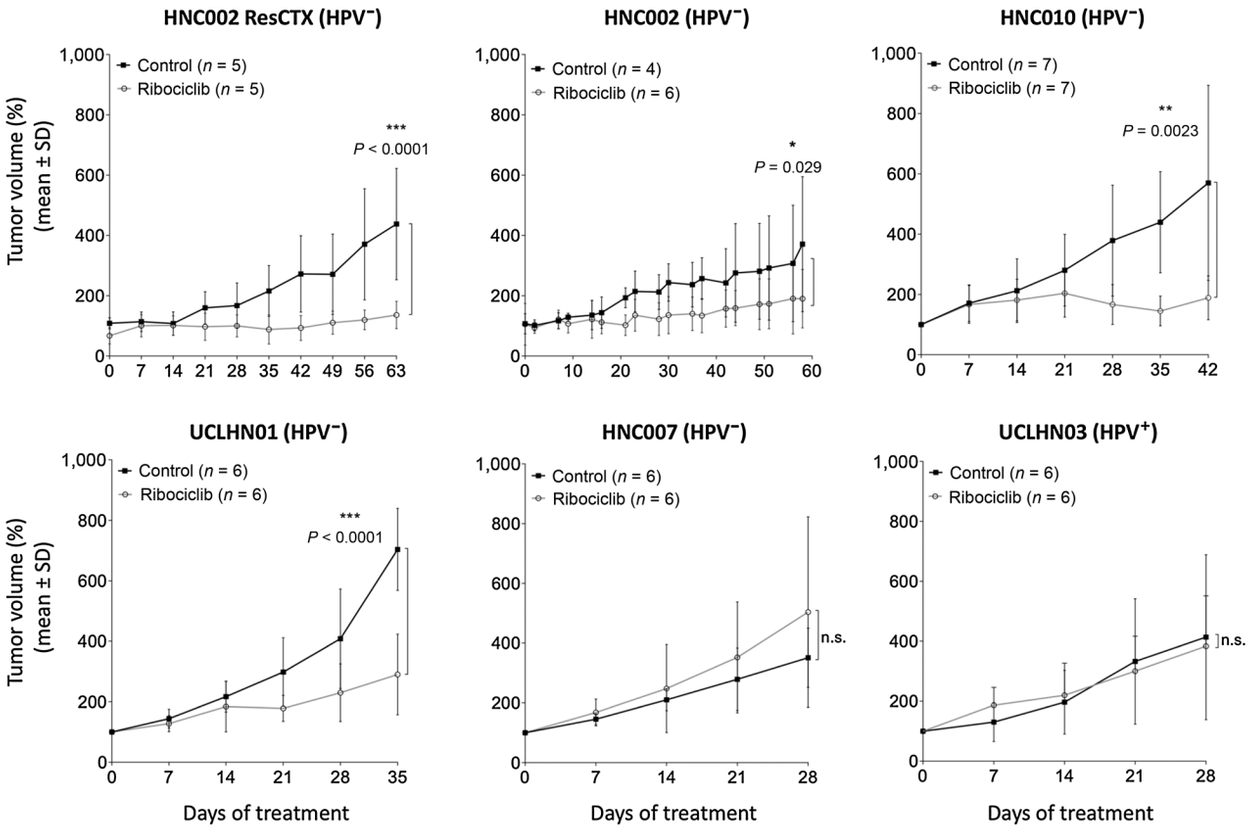

Figure 2.

Ribociclib activity was evaluated in six PDTX models: five HPV-negative and one HPV-positive. Mice received daily 100 mg/kg ribociclib (gray) or vehicle (black). n.s.: $P > 0.05$; $^{*}P < 0.05$; $^{**}P < 0.001$; $^{***}P < 0.0001$. n.s., no significance.

with the epithelial-like cells (CAL27, FaDu, Detroit-562, and SCC25; vimentin *P*: 0.0192, snail $P < 0.0001$; **Fig. 3B** and **C**). The protein expression level of slug and zeb1 did not vary between these two groups. In addition, in cells with epithelial-like morphology, e-cadherin is generally located in the membrane (19), as observed in all three sensitive cell lines by immunofluorescence (**Fig. 3D**), whereas e-cadherin was located in the cytoplasm of cell lines expressing a more mesenchymal phenotype.

These preliminary findings suggested that the mesenchymal cellular phenotype and epithelial-to-mesenchymal transition (EMT) could interfere with ribociclib activity. Therefore, we investigated this hypothesis in our cell lines using a migration assay (**Fig. 3E**). As expected, SCC9 and SCC15 cells showed higher migration abilities than FaDu, CAL27, Detroit-562, and SCC25 cells.

The level of expression of vimentin and e-cadherin proteins was then evaluated by immunochemistry in our six PDTX models. Neither the level of vimentin, nor that of e-cadherin, correlated with tumor sensitivity to ribociclib treatment in HPV-negative PDTX models (*P* of vimentin: 0.117, *P* of e-cadherin: 0.762; **Fig. 3F**).

Retinoblastoma protein intensity correlated with SCCHN tumor cell response to ribociclib

To verify that the proliferation inhibition observed in HPV-negative SCCHN cell lines was mediated by a target impairment of the CyclinD–CDK4–CDK6–Rb pathway, the expression of multiple cell-cycle regulatory proteins was evaluated by immunoblotting following ribociclib exposure (**Fig. 4A**). As expected, ribociclib treatment decreased pRb in HPV-negative cell lines and induced cyclin A downregulation. Cyclin A is a direct downstream target of E2F1-3 (20) and these results indicate the ability of Rb to mediate cell-cycle arrest. The levels of CDK4 and CDK6 expression were not influenced by ribociclib treatment.

A striking difference between HPV-positive and -negative SCCHN is the expression of Rb. In HPV-positive SCCHN cells, E7 oncoproteins induce Rb degradation (21), which may explain the resistance of SCCHN HPV-positive cells to ribociclib. In addition, p16 is overexpressed in HPV-positive SCCHN due to the loss of negative feedback induced by inactivation of Rb (22). Accordingly, Rb protein expression was not observed in UM-SCC47 and UPCI-SCC90 cell lines by immunoblotting assays while p16 expression was highly expressed (**Fig. 4A**). Interestingly, Rb and pRb were significantly less expressed in SCC9 and SCC15 (less sensitive cell lines) compared with the sensitive cell lines (Rb/GAPDH $P < 0.0001$, pRbS807-811/GAPDH $P = 0.0024$; **Fig. 4B**). Furthermore, the Rb protein expression level was inversely correlated with IC_{50} as calculated by the viability assay of the cell lines when treated with ribociclib ($r = -0.841$; **Fig. 4C**).

Similarly, the Rb protein expression level of the PDTX tumors correlated with tumor sensitivities to ribociclib treatment (HNC002-ResCTX, HNC002, HNC010 versus UCLHN01, HNC007, UCLHN03 $P = 0.0002$; **Fig. 4D**). HPV-negative PDTX models (HNC002ResCTX, HNC002, HNC010) with a higher Rb protein expression level [Rb Histoscore (H-score) mean ± SD = 274

Published OnlineFirst January 10, 2020; DOI: 10.1158/1535-7163.MCT-19-0695

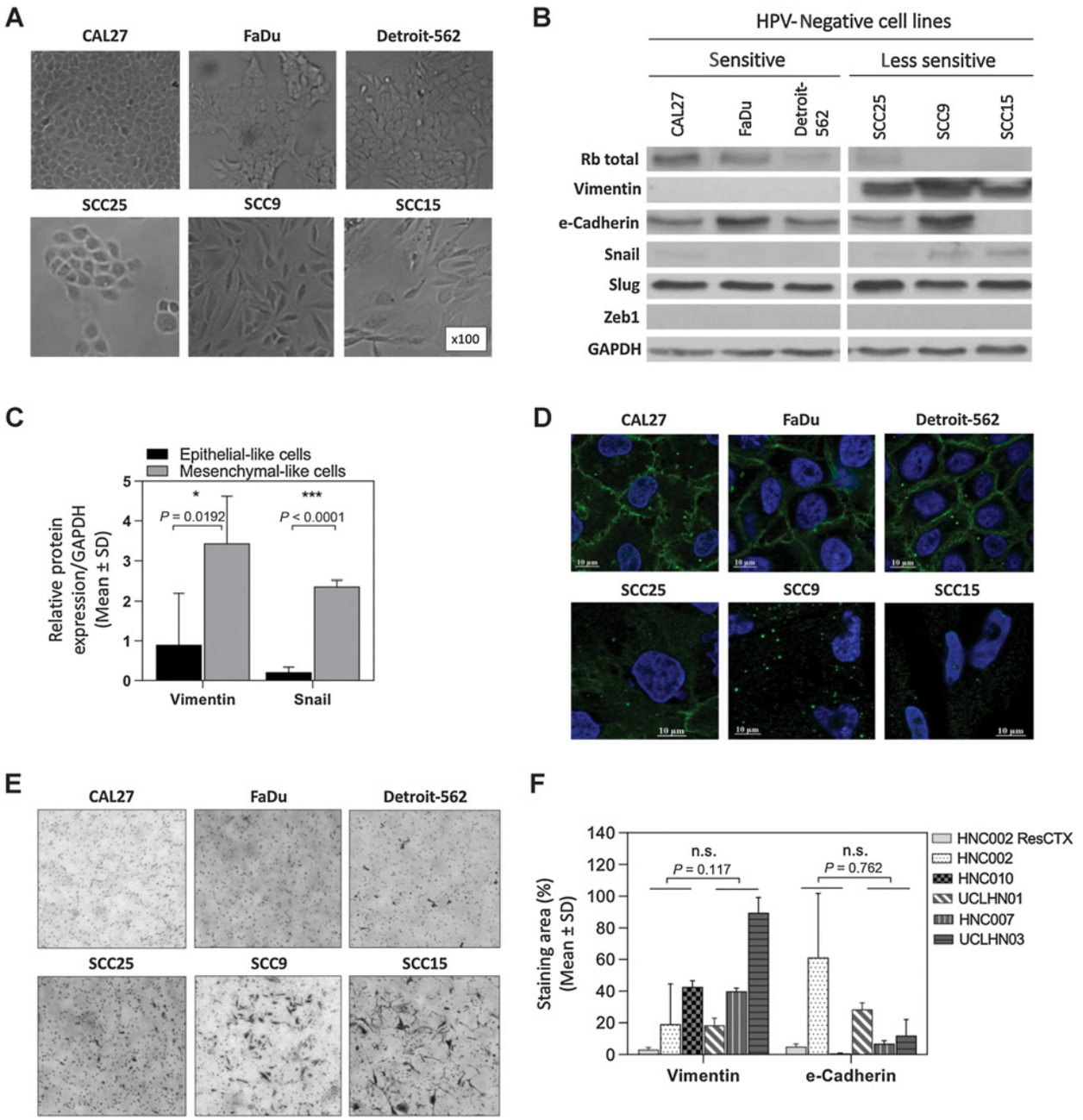

Figure 3.

EMT as a predictive biomarker of ribociclib resistance. **A,** Cell morphology of HPV-negative SCCHN cell lines. SCC9 and SCC15 cell lines presented a mesenchymal-like morphology. CAL27, FaDu, Detroit-562, and SCC25 cell lines presented an epithelial-like morphology. **B,** Protein expression of mesenchymal (vimentin, snail, slug, and zeb1) and epithelial (e-cadherin) markers in HPV-negative SCCHN human cell lines were analyzed by immunoblotting. **C,** The relative protein expressions of vimentin and snail normalized with GAPDH were compared between epithelial-like cells (CAL27, FaDu, Detroit-562, and SCC25) (black bars) and mesenchymal-like cells (SCC9 and SCC15; gray bars). Mean ± SD were obtained from three independent immunoblotting assays. **D,** Localization of e-cadherin (green) analyzed by immunofluorescence in the HPV-negative SCCHN cell lines. Nuclei are stained with DAPI (blue). **E,** Cell migration abilities were analyzed using the Boyden chamber transwell assay in the HPV-negative SCCHN cell lines. **F,** Protein expression levels of vimentin and e-cadherin were evaluated in the six PDTX models. Mean ± SD were obtained in three independent tumor/model using IHC assays. n.s.: $P > 0.05$; $^{*}P < 0.05$; $^{**}P < 0.001$; $^{***}P < 0.0001$. n.s., no significance.

± 16, 270 ± 18 and 274 ± 5, respectively] were more sensitive to ribociclib compared with the other models. The two HPV-negative PDTX models with a lower Rb protein expression level were less sensitive (UCLHN01, Rb H-score mean ± SD = 222 ± 8) or resistant (HNC007, Rb H-score mean ± SD = 134 ± 19) to ribociclib. The HPV-positive PDTX model (UCLHN03) was resistant to ribociclib and presented a low expression of Rb proteins (Rb H-score mean ± SD = 11 ± 11).

Published OnlineFirst January 10, 2020; DOI: 10.1158/1535-7163.MCT-19-0695

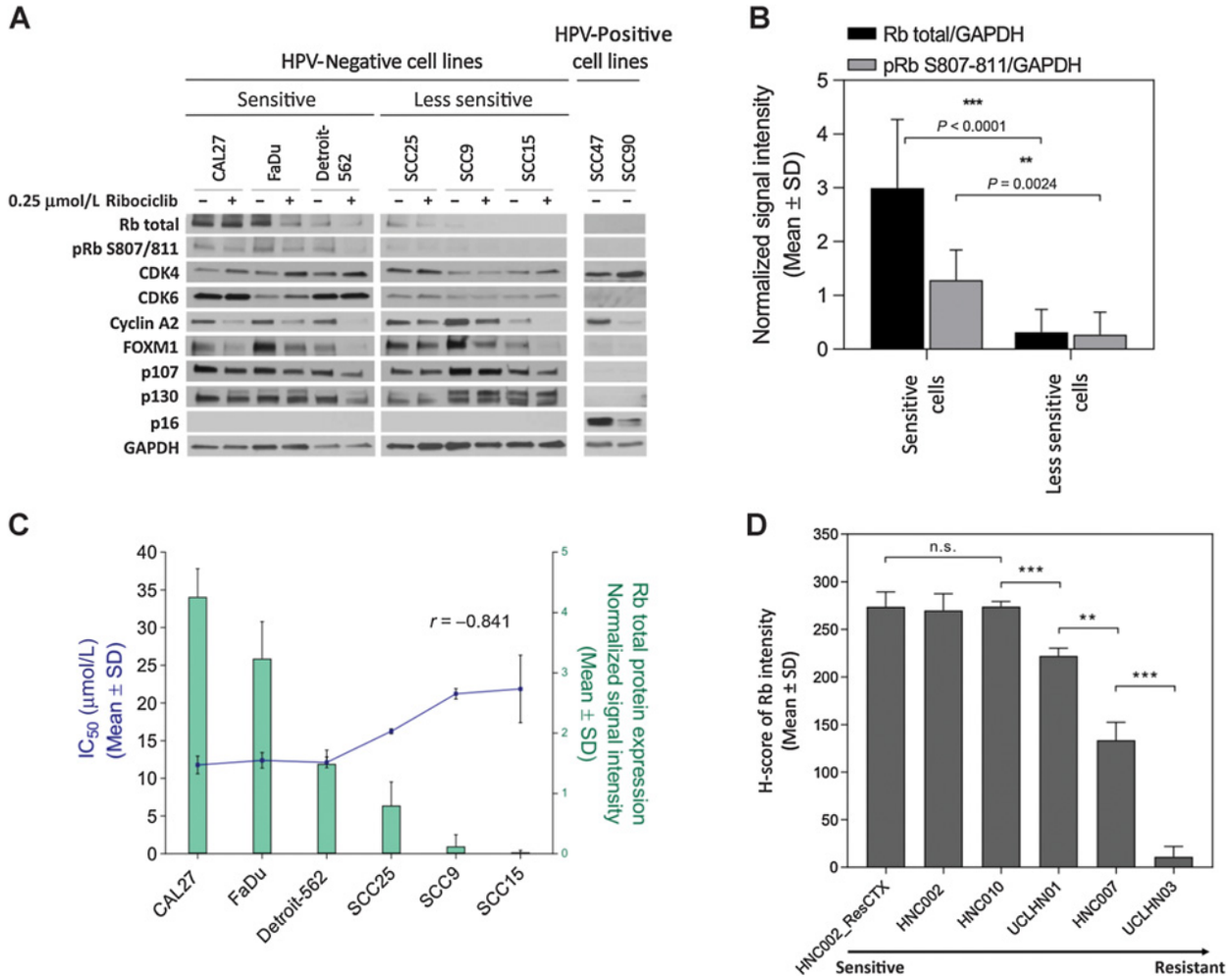

Figure 4.

Rb as a predictive biomarker of ribociclib response. **A,** The expression of proteins associated with the cell cycle was obtained by immunoblotting for the eight SCCHN cell lines. HPV-negative cell lines were treated for 24 hours with 0.25 µmol/L ribociclib. **B,** The relative protein expression of Rb (black bars) and pRbS807-811 (gray bars) normalized with GAPDH was compared between sensitive cell lines (CAL27, FaDu, Detroit-562) and less sensitive cell lines (SCC25, SCC9, SCC15). Mean ± SD were obtained from three independent immunoblotting assays. **C,** Rb total protein expression (green) was significantly downregulated in less sensitive compared with sensitive HPV-negative cell lines. Rb protein expression level (green) was inversely correlated with the IC_{50} (blue) of the cell lines when treated with ribociclib (r: −0.841). Mean ± SD were obtained from three independent immunoblotting assays and three independent MTT assays. **D,** Protein expression level of Rb was evaluated in six PDTX models and associated with tumor sensitivity to ribociclib. Rb protein intensity was represented with H-score. Mean ± SD were obtained in three independent tumor/model using immunochemistry assays. n.s.: > 0.05; $^{*}P < 0.05$; $^{**}P < 0.001$; $^{***}P < 0.0001$. n.s., no significance.

These data suggested that the Rb expression level might be correlated with ribociclib activity.

Retinoblastoma protein intensity alone is not sufficient to predict response to ribociclib treatment in all HPV-negative cell lines

To determine whether the presence of *RB1* is essential to induce cell-cycle arrest following ribociclib treatment, Rb-positive FaDu, CAL27, and Detroit-562 cells were transfected with siRNA targeting *RB1*, or nontargeting siRNA. After the incubation of CAL27 and FaDu cells with siRNA targeting *RB1*, ribociclib did not induce a statistically significant increase in the percentage of cells in G_0–G_1 phase. In contrast, in Detroit-562, ribociclib induced a significant G_0–G_1 cell-cycle arrest independently of Rb status (**Fig. 5A**). These findings suggest that molecular mechanisms other than Rb expression could be involved in cell-cycle arrest in the G_0–G_1 phase mediated by ribociclib in Detroit-562.

As hypothesis generating, a proteomic analysis was performed on Detroit-562 to highlight the mechanisms by which ribociclib induced cell-cycle arrest in Rb-deficient cells. Downregulation of known E2F1-3 targets was observed independently of Rb status after ribociclib treatment (**Fig. 5B**) and was confirmed by immunoblotting assays (**Fig. 5D**). Moreover, and independently of Rb status, ribociclib induced downregulation of the forkhead box M1 (FOXM1) protein and its downstream targets (**Fig. 5C** and **E**). It has been previously demonstrated that FOXM1 is a direct target of CDK4/6 and that it is implicated in cell-cycle regulation (23). In addition, Rb downregulation in Detroit-562 cells induced an increase of the FOXM1 protein level. Ribociclib-mediated FOXM1 downregulation independently of Rb status (**Fig. 5E**).

Published OnlineFirst January 10, 2020; DOI: 10.1158/1535-7163.MCT-19-0695

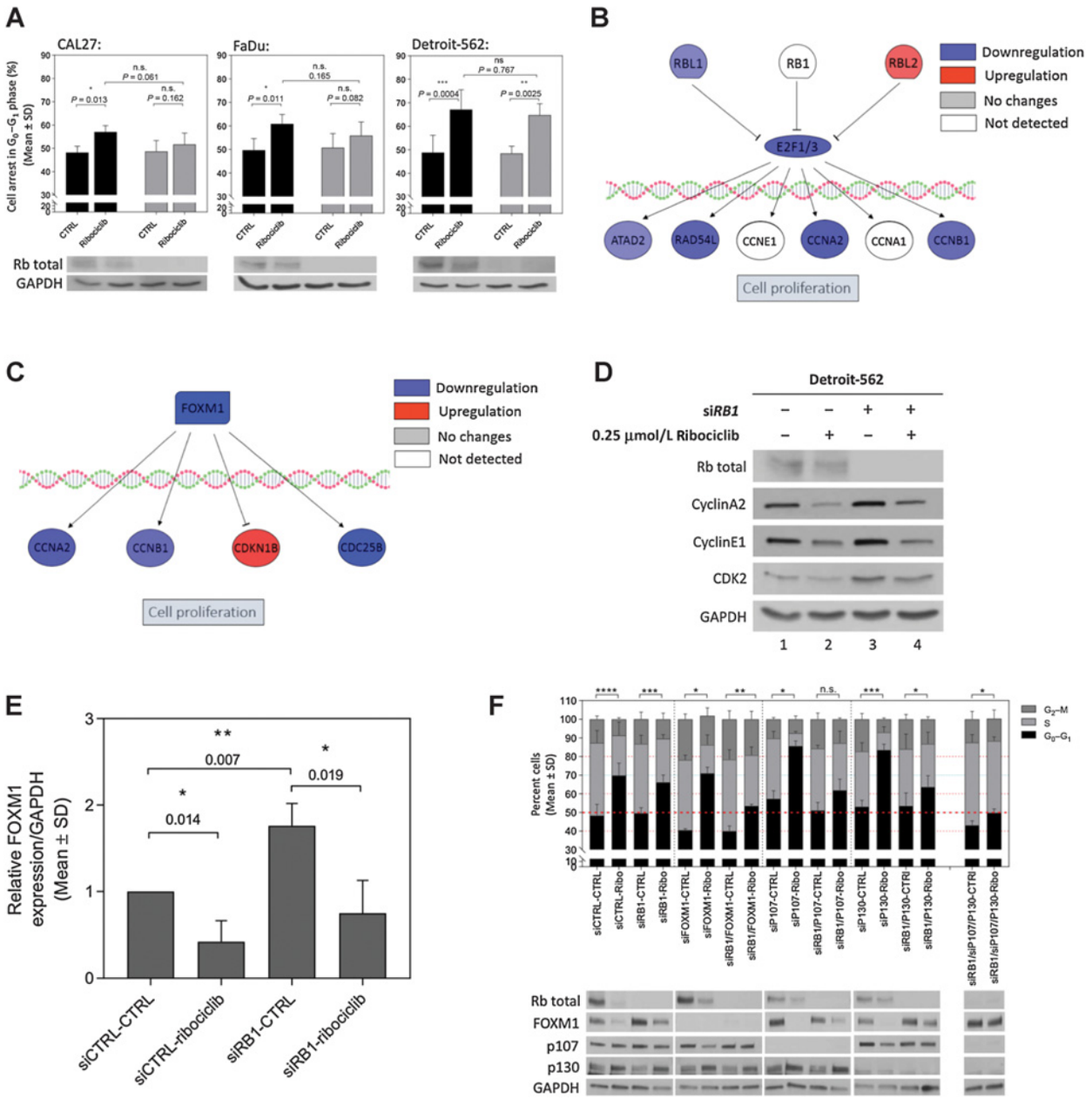

Figure 5.

Rb downregulation is not sufficient to induce ribociclib resistance in Detroit-562. p107, p130, and FOXM1 contribute to induce G_0–G_1 arrested mediated by ribociclib in this cell line. **A,** The percentage of cell arrest in G_0–G_1 after 72 hours incubation with nontargeting siRNA (siCTRL, black bars) or siRNA targeting *RB1* (si*RB1*, gray bars) following 24 hours of treatment with 0.25 µmol/L ribociclib or 0.1% DMSO (CTRL) in Detroit-562. Mean ± SD were obtained from three independent flow cytometry assays. Rb and GAPDH protein expression levels were obtained by immunoblotting. Proteomic analysis showed a downregulation of the protein expression of E2F1-3 and its known targets (**B**) and a downregulation of the protein expression of FOXM1 and its targets implicated in cell-cycle regulation (**C**). **D,** The level of expression of known E2F targets (cyclinA2, cyclinE1, and CDK2) was analyzed by immunoblotting assay in Detroit-562 after 72 hours incubation with siRNA targeting si*RB1* (lines 1 and 2) or nontargeting siRNA (lines 3 and 4), and then exposed to 0.25 µmol/L ribociclib (lines 2 and 4) or 0.1% DMSO/control for 24 hours (lines 1 and 3). **E,** FOXM1 protein expression levels were analyzed in Detroit-562 cell lines treated with nontargeting siRNA (siCTRL) or siRNA targeting *RB1* (si*RB1*) following 0.25 µmol/L ribociclib or 0.1% DMSO (CTRL). Mean ± SD were obtained from three independent immunoblotting assays. **F,** The percentage of cell arrest in G_0–G_1 after 72 hours incubation with siRNA(s) targeting *siFOXM1, siRB1* (Rb) + *siFOXM1, siRBL1* (p107), *siRB1* (Rb) + si*RBL1* (p107), *siRBL2* (p130), *siRB1* (Rb) + *RBL2* (p130), and *siRB1* (Rb) + *siRBL1* (p107) + *siRBL2* (p130), or nontargeting siRNA (siCTRL), and then exposed to 0.25 µmol/L ribociclib or 0.1% DMSO/control for 24 hours. Mean ± SD were obtained from three independent flow cytometry assays. Rb, p107, p130, FOXM1, and GAPDH protein expression levels were obtained by immunoblotting. n.s.: $P > 0.05$; $^{*}P < 0.05$; $^{**}P < 0.001$; $^{***}P < 0.0001$. n.s., no significance.

Published OnlineFirst January 10, 2020; DOI: 10.1158/1535-7163.MCT-19-0695

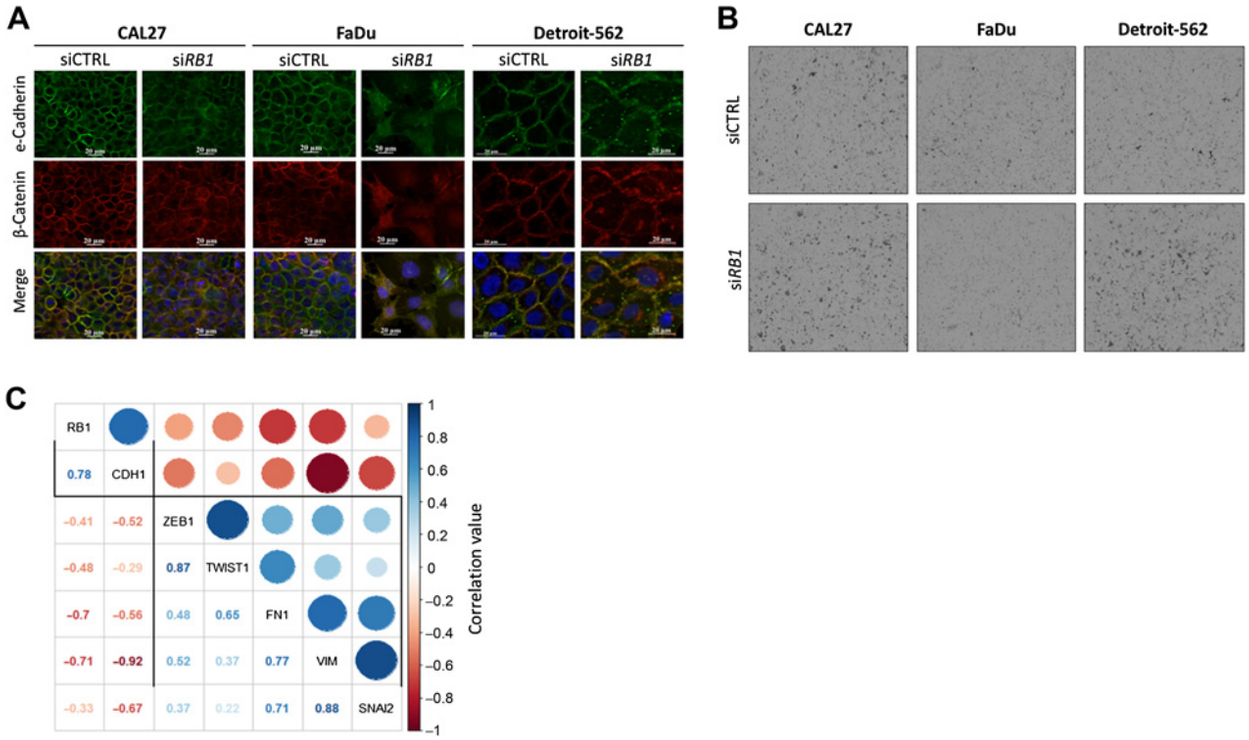

Figure 6.

The correlation between Rb protein expression and EMT-associated protein expressions. **A,** e-Cadherin (green) and β-catenin (red) localization after 72 hours of incubation with nontargeting siRNA (siCTRL) or siRNA targeting *RB1* (siRB1) in CAL27, FaDu, and Detroit-562 cell lines was obtained by immunofluorescence analysis. **B,** Cell migration abilities were analyzed using the Boyden chamber transwell assay in CAL27, FaDu, and Detroit-562 cell lines treated for 72 hours with nontargeting siRNA (siCTRL) or siRNA targeting *RB1* (siRB1). **C,** Pearson correlation between mRNA expression of *RB1*, epithelial marker (*CDH1*), and mesenchymal markers (*ZEB1, TWIST1, FN1, VIM,* and *SNAI2*) across CAL27, Detroit-562, SCC25, SCC9, and SCC15 cell lines. Positive and negative correlations are shown in blue and red, respectively. Color intensity and circle size are proportional to the correlation coefficient. Numerical values of the coefficients are represented in mirror. Patterns of variation were hierarchically clustered in two groups using Ward criterion.

To determine whether ribociclib could induce the regulation of E2F1-3 targets through Rb-homologs, p107 and p130, and cell-cycle arrest through FOXM1, we characterized our six HPV-negative cell lines for these proteins. p107, p130, and FOXM1 baseline protein expression levels did not correlate with the ribociclib IC_{50} of the SCCHN cell lines (**Fig. 4A**). Furthermore, to determine the role of p107, p130, and FOXM1 in cell-cycle regulation mediated by ribociclib, Detroit-562 cells were transfected for 72 hours with siRNA(s) targeting si*FOXM1*, si*RB1* + si*FOXM1*, si*RBL1* (p107), si*RB1* + si*RBL1*, si*RBL2* (p130), si*RB1* + si*RBL2* and si*RB1* + si*RBL1* + si*RBL2* or nontargeting siRNA, and then exposed to ribociclib or DMSO/control for 24 hours (**Fig. 5F**). Neither siRNA targeting *FOXM1, RBL1* or *RBL2* alone reduced the activity of ribociclib in Detroit-562 cell lines. The combination of siRNA targeting *RB1*, with either *FOXM1* or *RBL1* or *RBL2*, significantly decreased the percentage of cell arrest in the G_0–G_1 phase following ribociclib exposure compared with cells transfected with only one siRNA and treated with ribociclib (**Fig. 5F**). Moreover, ribociclib was less able to induce G_0–G_1 cell-cycle arrest in Detroit-562 when we simultaneously knockdowned Rb, p107, and p130, suggesting the redundancy of the role of these proteins in this cell line.

These results suggest that the level of Rb protein expression alone might not be sufficient to predict SCCHN cell response to ribociclib treatment in all cell lines, and that the transcriptional factor FOXM1, as well as other Rb family proteins, may also play a role.

Rb depletion is linked to EMT

To investigate whether Rb downregulation is linked with mesenchymal cell phenotype, we analyzed by immunofluorescence the localization of e-cadherin and β-catenin following Rb knockdown in epithelial-like cells (FaDu, CAL27, Detroit-562; refs. 24, 25). In CAL27, without treatment, e-cadherin and β-catenin were detected at cell-cell interfaces. After 72 hours of incubation with siRNA targeting *RB1*, surface e-cadherin and β-catenin staining decreased and became diffuse in the cytoplasm. Similar results were observed in FaDu and Detroit (**Fig 6A**).

Next, we investigated the capacity of Rb downregulation to induce cell mobility on epithelial-like cells. CAL27 and Detroit-562 cells led to an increase in cell migration abilities after 72 hours of incubation with siRNA targeting *RB1* (**Fig. 6B**). This was not observed in the FaDu cell line.

To further study the correlation between *RB1* expression and the EMT process, we analyzed mRNA expression by RNAseq in the five HPV-negative SCCHN cell lines (CAL27, Detroit-562, SCC25, SCC9, and SCC15). *CDH1* mRNA expression inversely correlated with EMT-associated genes such as *SNAI2, VIM, ZEB1, TWIST1*, and *FN1*, and together, these EMT-associated genes showed positive correlations.

Published OnlineFirst January 10, 2020; DOI: 10.1158/1535-7163.MCT-19-0695

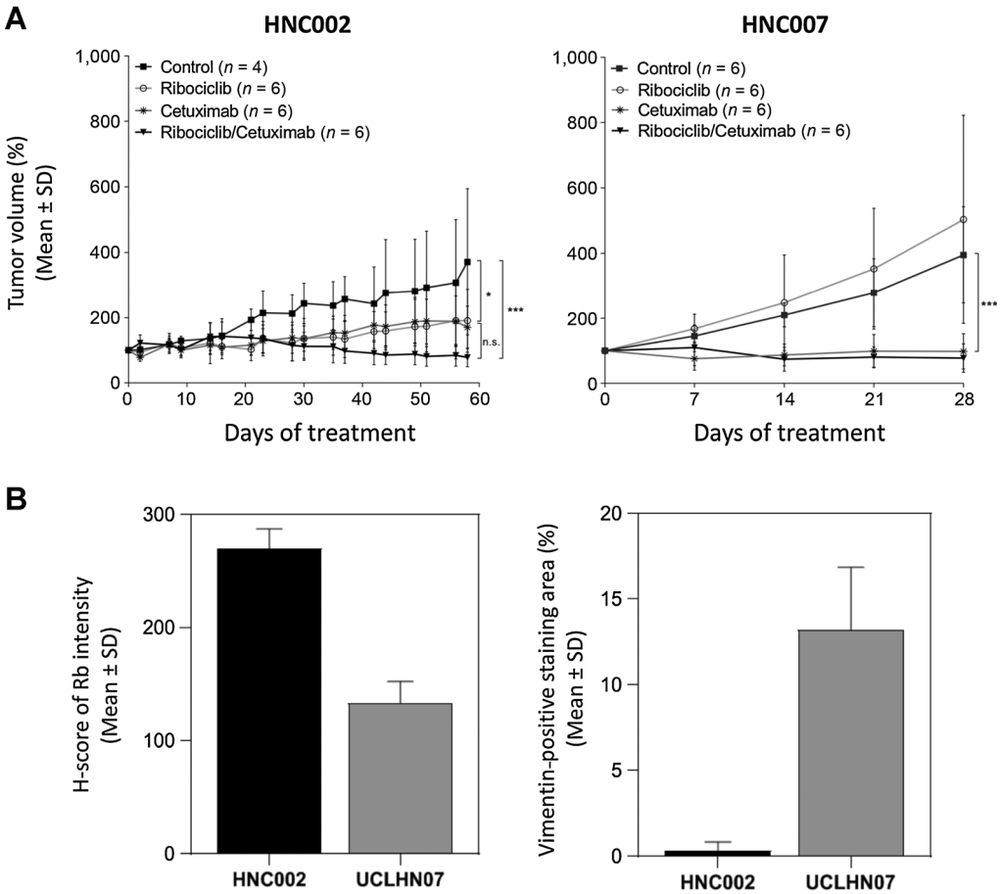

Figure 7.

Ribociclib, cetuximab, and ribociclib/cetuximab activities were evaluated in two HPV-negative SCCHN PDTX models. **A,** Mice received daily 100 mg/kg ribociclib, weekly 30 mg/kg cetuximab, the combination of ribociclib and cetuximab, or the vehicles. **B,** The protein expression level of Rb and vimentin was evaluated in HNC002 and UCLHN07 models. Rb protein intensity was represented with H-score. Vimentin expression was determined as percentage of stained area. Mean ± SD were obtained in three independent tumor/model using immunochemistry assays n.s.: $P > 0.05$; $^{*}P < 0.05$; $^{**}P < 0.001$; $^{***}P < 0.0001$. n.s., no significance.

Interestingly, a positive correlation between *RB1* and *CDH1* mRNA expression levels was observed (**Fig. 6C**). Conversely, a negative correlation was found between the gene expression levels of *RB1* and EMT-associated genes.

These results suggested an inverse correlation between the expression of *RB1* and markers of EMT.

The combination of ribociclib and cetuximab might be beneficial in HPV-negative SCCHN

Given that ribociclib is cytostatic, the activity of ribociclib combined with cetuximab was investigated in two HPV-negative PDTX models: one ribociclib- and cetuximab-sensitive model harboring a high expression of Rb and a low expression of vimentin (HNC002), and one ribociclib-resistant and cetuximab-sensitive model harboring a low expression of Rb and a high expression of vimentin (HNC007; **Fig. 7A** and **B**). In HNC002, the combination of cetuximab and ribociclib induced tumor size regression, but the mean tumor size was not significantly different when treated with the combination compared with cetuximab or ribociclib alone (cetuximab vs. combination $P = 0.365$, ribociclib vs. combination $P = 0.195$). In HNC007, the combination of cetuximab and ribociclib induced similar tumor size stabilization compared with cetuximab alone (cetuximab vs. combination $P > 0.999$).

Discussion

We showed that ribociclib induced cell-cycle arrest in HPV-negative SCCHN cell lines and delayed tumor cell growth in some HPV-negative SCCHN PDTX models. Ribociclib has no activity in HPV-positive SCCHN models. We also showed that EMT and the Rb-family proteins might play, to some degree, a predictive role in some HPV-negative SCCHN preclinical models.

We found in our *in vitro* and *in vivo* models a positive correlation between the level of Rb protein expression and the activity of ribociclib. The value of Rb to predict response to CDK4/6 inhibition is debated with conflicting results. We found that Rb downregulation in Detroit-562 did not induce ribociclib resistance. One possible explanation is the contribution of p107 and p130, the retinoblastoma-related proteins. It has been demonstrated that in Rb-deficient cells, p107 and p130 have overlapping functions with Rb to regulate the release of E2Fs (26). The fact that p107 and p130 are also phosphorylated and regulated by CDK4/6–cyclin D complexes (23) provides an

Published OnlineFirst January 10, 2020; DOI: 10.1158/1535-7163.MCT-19-0695

explanation as to why retinoblastoma knockdown in the Detroit-562 cell line is not sufficient to induce resistance to ribociclib. Rb, p107, or p130 downregulation in Detroit-562 cells did not reduce the activity of ribociclib when each of these proteins was downregulated separately. When Rb, p107, and p130 were downregulated at the same time, we saw reduced activity of ribociclib in Detroit-562. These observations support the redundancy of functions of these three homologs in Detroit-562.

We also observed in Detroit-562 cells that ribociclib induced the downregulation of FOXM1 transcriptional factor. This downregulation of FOXM1, mediated by ribociclib, was expected since hypophosphorylated Rb mediates *FOXM1* mRNA repression (27). However, independently of Rb status, FOXM1 can be stabilized and activated directly by CDK4/6–cyclin D complexes (23), which could explain why we observed FOXM1 downregulation following ribociclib treatment even in Rb-deficient Detroit-562 cells. In addition, the loss of Rb has been shown to induce FOXM1 activation in bladder cells, and FOXM1 proteins expression conferred resistance to CDK4/6 inhibition only in Rb-mutant cells (28). We also observed a significant increase in the FOXM1 protein level following Rb downregulation by siRNA in Detroit-562 cells. All these observations suggest that, in addition to p107 and p130, FOXM1 could also play a role in cell-cycle progression control induced by CDK4/6–cyclin D complexes independently of Rb status. It should be noted that Detroit-562 harbors activating *PIK3CA* mutation that could activate FOXM1 (29). Besides the potential role of the Rb-protein family and FOXM1, we also cannot exclude other off-target effects of ribociclib, outlining the difficulties in identifying predictive biomarkers with such compounds. Altogether, these findings highlight the complexity of cell-cycle regulation. This could explain why most clinical studies have failed to associate alterations of the Cyclin D–CDK4–CDK6–Rb pathway with CDK4/6 inhibitor efficacy, although it has been widely investigated in breast cancer (30). Here, we demonstrated that different proteins involved in the cell cycle (Rb, p107, p130, and FOXM1) have possible overlapping functions. This suggests that a single biomarker will not be able to predict ribociclib activity, but that we will have to consider multiple molecular mechanisms. The PALOMA-3 phase III trial found a correlation between a high expression of *CCNE1* and breast cancer tumor resistance to palbociclib (31). This correlation was not observed in our SCCHN cell lines (Supplementary Fig. S2) and *CCNE1* alterations are not frequent in SCCHN (32).

We observed that cell lines harboring a mesenchymal phenotype (SCC9 and SCC15) and EMT features were less sensitive to ribociclib than those with an epithelial phenotype (FaDu, CAL27, Detroit-562). EMT has frequently been associated with cancer cell resistance to various anticancer drugs (33, 34). The mechanisms implicated include the ability of EMT-associated genes to attenuate cell-cycle progression and the ability to repress transcriptional genes associated with proapoptotic activities (35, 36). However, in our PDTX models, we found that ribociclib has significant activity in the HNC010 model that expressed a similar level of vimentin as the resistant HPV-negative model (HNC007). HNC010 expressed a high level of Rb, suggesting that EMT alone is not sufficient to induce ribociclib resistance, particularly when EMT is not associated with a low level of Rb expression. Furthermore, EMT can be reversible (37), and sometimes cancer cells can be in different states of differentiation with hybrid phenotypes (38). In addition, SCCHN is highly heterogeneous and that could add a layer of complexity (39, 40).

In SCCHN, Rb loss is associated with poor prognosis (41). It has been previously demonstrated that Rb is critical for cell proliferation control but that it could also play a role in cancer cell invasion and the apparition of distant metastasis (42, 43). In our SCCHN cell lines, we observed that Rb downregulation mediated e-cadherin and β-catenin internalization from membrane to cytoplasm, one characteristic of the EMT process (25). Moreover, Rb loss promoted the invasiveness of two SCCHN epithelial-like cell lines, Detroit-562 and CAL27. Similarly, Arima and colleagues (44) showed that Rb can directly or indirectly mediate e-cadherin expression in MCF7 breast cancer cells. They observed that Rb loss promoted cell mobility and induced slug and zeb-1 expression, two EMT-related proteins. These findings, and our observations, confirm that Rb may play a role in maintaining the epithelial-like phenotype, and that Rb loss could be associated with EMT and cell invasion.

All our findings suggest that CDK4/6 inhibitors should be investigated in patients with HPV-negative SCCHN with a high Rb expression and epithelial phenotype. Although these biomarkers are clearly not optimal, as this work has demonstrated, they may enrich the population that is more likely to benefit from a CDK4/6 inhibitor.

In vivo, ribociclib has only a cytostatic effect with no tumor shrinkage observed in our PDTX models. This supports the investigation of CDK4/6 inhibitors in combination with other treatments. In breast cancer, it has been shown that CDK4/6 inhibitors improve outcomes in combination with hormone therapy (31, 45). The best combination partner in SCCHN still needs to be identified. Preclinical studies have found, *in vitro* or *in vivo* synergy between CDK4/6 inhibitors with either PI3K pathway inhibitors in *PIK3CA*-mutated cancer cells, or lapatinib and afatinib, or immune checkpoint inhibitors (46–49). Recently, a randomized phase II study failed to demonstrate the superiority of the cetuximab/palbociclib combination over cetuximab single agent in recurrent SCCHN (11). However, this study was performed in an unselected HPV-negative SCCHN population. Therefore, a better understanding of the molecular mechanisms involved in treatment response and/or resistance is needed to optimally select patients with SCCHN who could benefit from CDK4/6 inhibitors combined with cetuximab. In HNC002, the ribociclib and cetuximab combination induced some degree of tumor regression that could not be achieved with cetuximab or ribociclib when administered as a single agent. HNC002 harbors high Rb expression and low vimentin expression, supporting the hypothesis that this combination might have some degree of activity in this molecular subgroup. However, more preclinical work is needed to further assess the potential of this treatment combination before continuing its investigation in the clinic.

We have demonstrated that ribociclib has a cytostatic effect in some HPV-negative SCCHN preclinical models. Further preclinical investigations and biomarker-driven clinical trials are needed to refine the predictive value of potential biomarkers and to identify the best combination partner.

Disclosure of Potential Conflicts of Interest

J.-P. Machiels is a consultant/advisory board member at Novartis and MSD. No potential conflicts of interest were disclosed by the other authors.

Authors' Contributions

Conception and design: G. van Caloen, S. Schmitz, D. Vertommen, J.-P. Machiels
Development of methodology: G. van Caloen, S. Schmitz, D. Vertommen, J.-P. Machiels
Acquisition of data (provided animals, acquired and managed patients, provided facilities, etc.): G. van Caloen, S. Schmitz, X. Caignet, S.P.D. Ruys, D. Vertommen, J.-P. Machiels
Analysis and interpretation of data (e.g., statistical analysis, biostatistics, computational analysis): G. van Caloen, S. Schmitz, M. El Baroudi, S.P.D. Ruys, P.P. Roger, D. Vertommen, J.-P. Machiels

Writing, review, and/or revision of the manuscript: G. van Caloen, S. Schmitz, M. El Baroudi, S.P.D. Ruys, P.P. Roger, D. Vertommen, J.-P. Machiels
Administrative, technical, or material support (i.e., reporting or organizing data, constructing databases): G. van Caloen, S. Schmitz
Study supervision: S. Schmitz, J.-P. Machiels

Acknowledgments

The authors wish to thank Aileen Eiszele for writing and editorial assistance, Eric Raspe for critical review of the manuscript, and Caroline Bouzin. Gabrielle van Caloen is a research fellow supported by a grant from the Belgian National Research Fund (Télévie/FNRS N22824344). This study was also financed by grants from the Belgian National Research Fund (FRSM 2013), Fondation Saint-Luc (Cliques universitaires Saint-Luc, Brussels), Fondation Louvain (UCLouvain), Fondation « Keeping me alive », and WALInnov 2017-02 (CICLIBTEST).

The costs of publication of this article were defrayed in part by the payment of page charges. This article must therefore be hereby marked *advertisement* in accordance with 18 U.S.C. Section 1734 solely to indicate this fact.

Received July 15, 2019; revised November 6, 2019; accepted January 3, 2020; published first January 10, 2020.

References

1. Bray F, Ren JS, Masuyer E, Ferlay J. Global estimates of cancer prevalence for 27 sites in the adult population in 2008. Int J Cancer 2013;132:1133–45.
2. Curado MP, Boyle P. Epidemiology of head and neck squamous cell carcinoma not related to tobacco or alcohol. Curr Opin Oncol 2013;25:229–34.
3. Taberna M, Mena M, Pavon MA, Alemany L, Gillison ML, Mesia R. Human papillomavirus-related oropharyngeal cancer. Ann Oncol 2017;28: 2386–98.
4. Gregoire V, Lefebvre JL, Licitra L, Felip E. EHNS-ESMO-ESTRO Guidelines Working Group. Squamous cell carcinoma of the head and neck: EHNS-ESMO-ESTRO clinical practice guidelines for diagnosis, treatment and follow-up. Ann Oncol 2010;21 Suppl 5:v184–6.
5. Vermorken JB, Mesia R, Rivera F, Remenar E, Kawecki A, Rottey S, et al. Platinum-based chemotherapy plus cetuximab in head and neck cancer. N Engl J Med 2008;359:1116–27.
6. Cramer JD, Burtness B, Le QT, Ferris RL. The changing therapeutic landscape of head and neck cancer. Nat Rev Clin Oncol 2019;16:669–83.
7. Gonzalez SL, Stremlau M, He X, Basile JR, Munger K. Degradation of the retinoblastoma tumor suppressor by the human papillomavirus type 16 E7 oncoprotein is important for functional inactivation and is separable from proteasomal degradation of E7. J Virol 2001;75:7583–91.
8. Cancer Genome Atlas Network. Comprehensive genomic characterization of head and neck squamous cell carcinomas. Nature 2015;517:576–82.
9. Seront E, Schmitz S, Papier M, van Maanen A, Henry S, Lonchay C, et al. Phase 1 study evaluating the association of the cyclin-dependent kinase 4/6 inhibitor ribociclib and cetuximab in recurrent/metastatic p16-negative squamous cell carcinoma of the head and neck. Front Oncol 2019;9:155.
10. Adkins D, Oppelt PJ, Ley JC, Trinkaus K, Neupane PC. Multicenter phase II trial of palbociclib, a selective cyclin dependent kinase (CDK) 4/6 inhibitor, and cetuximab in platinum-resistant HPV unrelated (-) recurrent/metastatic head and neck squamous cell carcinoma (RM HNSCC). J Clin Oncol 2018;36: 6008.
11. Adkins D, Lin JC, Gesualda Sacco A, Ley JC, Oppelt PJ, Shen Q, et al. Palbociclib plus cetuximab versus placebo plus cetuximab in platinum-resistant, cetuximab-naive, HPV-unrelated head and neck cancer: a double-blind randomized phase II trial (PALATINUS). J Clin Oncol 37:15s, 2019 (suppl; abstr 6013).
12. Schneider K, Bol V, Gregoire V. Lack of differences in radiation-induced immunogenicity parameters between HPV-positive and HPV-negative human HNSCC cell lines. Radiother Oncol 2017;124:411–7.
13. Mignion L, Schmitz S, Michoux N, Caignet X, Goebbels RM, Bol A, et al. 2'-deoxy-2'-[18F] fluoro-D-glucose positron emission tomography, diffusion-weighted magnetic resonance imaging, and choline spectroscopy to predict the activity of cetuximab in tumor xenografts derived from patients with squamous cell carcinoma of the head and neck. Oncotarget 2018;9:28572–85.
14. Martin D, Abba MC, Molinolo AA, Vitale-Cross L, Wang Z, Zaida M, et al. The head and neck cancer cell oncogenome: a platform for the development of precision molecular therapies. Oncotarget 2014;5:8906–23.
15. Bouzin C, Saini ML, Khaing KK, Ambroise J, Marbaix E, Gregoire V, et al. Digital pathology: elementary, rapid and reliable automated image analysis. Histopathology 2016;68:888–96.
16. Arts IS, Ball G, Leverrier P, Garvis S, Nicolaes V, Vertommen D, et al. Dissecting the machinery that introduces disulfide bonds in Pseudomonas aeruginosa. MBio 2013;4:e00912–3.
17. Anders S, Huber W. Differential expression analysis for sequence count data. Genome Biol 2010;11:R106.
18. Wei T, Simko V. R Package "corrplot": visualization of a correlation matrix (version 0.84); 2017. Available from: https://github.com/taiyun/corrplot.
19. Halbleib JM, Nelson WJ. Cadherins in development: cell adhesion, sorting, and tissue morphogenesis. Genes Dev 2006;20:3199–214.
20. Roskoski R Jr. Cyclin-dependent protein serine/threonine kinase inhibitors as anticancer drugs. Pharmacol Res 2019;139:471–88.
21. Leemans CR, Braakhuis BJ, Brakenhoff RH. The molecular biology of head and neck cancer. Nat Rev Cancer 2011;11:9–22.
22. Narisawa-Saito M, Kiyono T. Basic mechanisms of high-risk human papillomavirus-induced carcinogenesis: roles of E6 and E7 proteins. Cancer Sci 2007;98: 1505–11.
23. Anders L, Ke N, Hydbring P, Choi YJ, Widlund HR, Chick JM, et al. A systematic screen for CDK4/6 substrates links FOXM1 phosphorylation to senescence suppression in cancer cells. Cancer Cell 2011;20:620–34.
24. Son H, Moon A. Epithelial-mesenchymal transition and cell invasion. Toxicol Res 2010;26:245–52.
25. Howard S, Deroo T, Fujita Y, Itasaki N. A positive role of cadherin in Wnt/beta-catenin signalling during epithelial-mesenchymal transition. PLoS One 2011;6: e23899.
26. Lee EY, Cam H, Ziebold U, Rayman JB, Lees JA, Dynlacht BD. E2F4 loss suppresses tumorigenesis in Rb mutant mice. Cancer Cell 2002;2:463–72.
27. Major ML, Lepe R, Costa RH. Forkhead box M1B transcriptional activity requires binding of Cdk-cyclin complexes for phosphorylation-dependent recruitment of p300/CBP coactivators. Mol Cell Biol 2004;24:2649–61.
28. Rubio C, Martinez-Fernandez M, Segovia C, Lodewijk I, Suarez-Cabrera C, Segrelles C, et al. Cdk4/6-inhibitor as a novel therapeutic approach for advanced bladder cancer independently of RB1 status. Clin Cancer Res 2018;25:390–402.
29. Gomes AR, Zhao F, Lam EW. Role and regulation of the forkhead transcription factors FOXO3a and FOXM1 in carcinogenesis and drug resistance. Chin J Cancer 2013;32:365–70.
30. van Caloen G, Machiels JP. Potential role of cyclin-dependent kinase 4/6 inhibitors in the treatment of squamous cell carcinoma of the head and neck. Curr Opin Oncol 2019;31:122–30.
31. Turner NC, Liu Y, Zhu Z, Loi S, Colleoni M. Cyclin E1 (CCNE1) expression associates with benefit from palbociclib in metastatic breast cancer (MBC) in the PALOMA3 trial. Cancer Res 2018;78:1169–78.
32. Stransky N, Egloff AM, Tward AD, Kostic AD, Cibulskis K, Sivachenko A, et al. The mutational landscape of head and neck squamous cell carcinoma. Science 2011;333:1157–60.
33. Huang J, Li H, Ren G. Epithelial-mesenchymal transition and drug resistance in breast cancer (review). Int J Oncol 2015;47:840–8.
34. Du B, Shim JS. Targeting epithelial-mesenchymal transition (EMT) to overcome drug resistance in cancer. Molecules 2016;21. doi: 10.3390/molecules21070965.
35. Vega S, Morales AV, Ocana OH, Valdes F, Fabregat I, Nieto MA. Snail blocks the cell cycle and confers resistance to cell death. Genes Dev 2004;18:1131–43.
36. Kajita M, McClinic KN, Wade PA. Aberrant expression of the transcription factors snail and slug alters the response to genotoxic stress. Mol Cell Biol 2004; 24:7559–66.
37. Zhang Y, Weinberg RA. Epithelial-to-mesenchymal transition in cancer: complexity and opportunities. Front Med 2018;12:361–73.
38. Jolly MK, Boareto M, Huang B, Jia D, Lu M, Ben-Jacob E, et al. Implications of the hybrid epithelial/mesenchymal phenotype in metastasis. Front Oncol 2015;5:155.
39. Canning M, Guo G, Yu M, Myint C, Groves MW, Byrd JK, et al. Heterogeneity of the head and neck squamous cell carcinoma immune landscape and its impact on immunotherapy. Front Cell Dev Biol 2019;7:52.
40. Leemans CR, Snijders PJF, Brakenhoff RH. The molecular landscape of head and neck cancer. Nat Rev Cancer 2018;18:269–82.

41. Beck TN, Golemis EA. Genomic insights into head and neck cancer. Cancers Head Neck 2016;1. doi: 10.1186/s41199-016-0003-z.
42. Sellers WR, Kaelin WG Jr. Role of the retinoblastoma protein in the pathogenesis of human cancer. J Clin Oncol 1997;15:3301–12.
43. Hui AM, Li X, Makuuchi M, Takayama T, Kubota K. Over-expression and lack of retinoblastoma protein are associated with tumor progression and metastasis in hepatocellular carcinoma. Int J Cancer 1999;84:604–8.
44. Arima Y, Inoue Y, Shibata T, Hayashi H, Nagano O, Saya H, et al. Rb depletion results in deregulation of E-cadherin and induction of cellular phenotypic changes that are characteristic of the epithelial-to-mesenchymal transition. Cancer Res 2008;68:5104–12.
45. Hortobagyi GN, Stemmer SM, Burris HA, Yap YS, Sonke GS, Paluch-Shimon S, et al. Updated results from MONALEESA-2, a phase III trial of first-line ribociclib plus letrozole versus placebo plus letrozole in hormone receptor-positive, HER2-negative advanced breast cancer. Ann Oncol 2018; 29:1541–7.
46. Goel S, DeCristo MJ, Watt AC, BrinJones H, Sceneay J, Li BB, et al. CDK4/6 inhibition triggers anti-tumour immunity. Nature 2017;548:471–5.
47. Pernas S, Tolaney SM, Winer EP, Goel S. CDK4/6 inhibition in breast cancer: current practice and future directions. Ther Adv Med Oncol 2018;10. doi: 10.1177/1758835918786451.
48. Knudsen ES, Witkiewicz AK. The strange case of CDK4/6 inhibitors: mechanisms, resistance, and combination strategies. Trends Cancer 2017; 3:39–55.
49. Gul A, Leyland-Jones B, Dey N, De P. A combination of the PI3K pathway inhibitor plus cell cycle pathway inhibitor to combat endocrine resistance in hormone receptor-positive breast cancer: a genomic algorithm-based treatment approach. Am J Cancer Res 2018;8:2359–76.

Published OnlineFirst January 10, 2020; DOI: 10.1158/1535-7163.MCT-19-0695

Molecular Cancer Therapeutics

Preclinical Activity of Ribociclib in Squamous Cell Carcinoma of the Head and Neck

Gabrielle van Caloen, Sandra Schmitz, Mariama El Baroudi, et al.

Mol Cancer Ther 2020;19:777-789. Published OnlineFirst January 10, 2020.